

Chiral interactions up to N³LO and nuclear saturation

C. Drischler,^{1,2,*} K. Hebeler,^{1,2,†} and A. Schwenk^{1,2,3,‡}

¹*Institut für Kernphysik, Technische Universität Darmstadt, 64289 Darmstadt, Germany*

²*ExtreMe Matter Institute EMMI, GSI Helmholtzzentrum für Schwerionenforschung GmbH, 64291 Darmstadt, Germany*

³*Max-Planck-Institut für Kernphysik, Saupfercheckweg 1, 69117 Heidelberg, Germany*

We present an efficient Monte-Carlo framework for perturbative calculations of infinite nuclear matter based on chiral two-, three-, and four-nucleon interactions. The method enables the incorporation of all many-body contributions in a straightforward and transparent way, and makes it possible to extract systematic uncertainty estimates by performing order-by-order calculations in the chiral expansion as well as the many-body expansion. The versatility of this new framework is demonstrated by applying it to chiral low-momentum interactions, exhibiting a very good many-body convergence up to fourth order. Following these benchmarks, we explore new chiral interactions up to next-to-next-to-next-to-leading order (N³LO). Remarkably, simultaneous fits to the triton and to saturation properties can be achieved, while all three-nucleon low-energy couplings remain natural. The theoretical uncertainties of nuclear matter are significantly reduced when going from next-to-next-to-leading order to N³LO.

Introduction.—Recent calculations of medium-mass and heavy nuclei have demonstrated the importance of realistic saturation properties of infinite matter for nuclear forces derived within chiral effective field theory (EFT) [1–5]. While most nucleon-nucleon (NN) and three-nucleon (3N) interactions fitted to only two- and few-body observables are able to predict light nuclei in agreement with experimental data, the theoretical uncertainties tend to increase with increasing mass number $A \gtrsim 16$ (see, e.g., Ref. [6]) and significant discrepancies to experiment can be found for properties of heavy nuclei [7]. There have been efforts to include properties of heavier nuclei in the optimization of chiral nuclear forces [1]. Such interactions tend to exhibit more realistic saturation properties of nuclear matter and also show improved agreement with experiment for energies and radii of medium-mass and heavy nuclei [2, 8–10]. However, the explicit incorporation of nuclear matter properties in the optimization process of nuclear forces has not been feasible so far due to the lack of computational efficiency of such calculations.

Nuclear matter has been studied based on chiral NN and 3N interactions within coupled-cluster theory [11], quantum Monte Carlo methods [12–14], the self-consistent Green’s function method [15], and many-body perturbation theory (MBPT) [16–24]. The advantages of MBPT are its computational efficiency as well as the possibility to estimate many-body uncertainties by comparing results at different orders. These factors are important for future optimizations of next-generation chiral interactions using nuclear-matter properties. So far, MBPT for infinite matter has only been applied up to third order including also the particle-hole channels [20, 24], where N²LO 3N contributions beyond Hartree-Fock have been included in terms of normal-ordered two-body interactions [22, 25, 26]. There remain however significant challenges, especially regarding the role of higher-order particle-hole vs. particle-particle or hole-hole contributions as well as the inclusion of 3N interactions at N³LO beyond Hartree-Fock [18, 23].

Novel framework.—In this Letter, we present a new Monte-Carlo framework for MBPT which is tailored to address these challenges. We perform our calculations directly in a single-particle product basis $|\mathbf{k}_i \sigma_i \tau_i\rangle$, without needing involved partial-wave decompositions. Tracing over spin $|\sigma_i\rangle$ and isospin states $|\tau_i\rangle$ of each particle with label i is fully automated, whereas the multidimensional integrals over the momenta \mathbf{k}_i are computed efficiently using adaptive Monte-Carlo algorithms [27–29]. This makes implementing arbitrary energy diagrams straightforward (including particle-hole contributions), even up to high orders in MBPT, while approximations in normal ordering are not needed anymore. However, it is well known that the number of diagrams at each order increases rapidly, with 3, 39, and 840 at third, fourth, and fifth order for NN-only interactions [30, 31]. Within our Monte-Carlo framework, a manual implementation of these would be feasible but still tedious and at least inefficient. We therefore developed an automatic code generator based on the analytic expression of a given diagram. The output in C++ is transparent, very compact and well readable, including dynamically generated comments.

In addition, we developed a general method to represent chiral interactions exactly as matrices in spin-isospin space, where the matrix elements are analytic functions of the single-particle momenta \mathbf{k}_i in the programming language C++. The automated generation of these interaction matrices is close to the operatorial definition of chiral forces [32–39], which we implemented with nonlocal regulators up to N³LO. Higher orders [40–42] can be included accordingly without the need of an involved partial-wave decomposition [43]. For the incorporation of NN interactions whose operatorial structure is not directly accessible (e.g., renormalization-group evolved potentials), we sum the contributions from all partial-wave channels for each Monte-Carlo sampling point. This step can also be performed very efficiently.

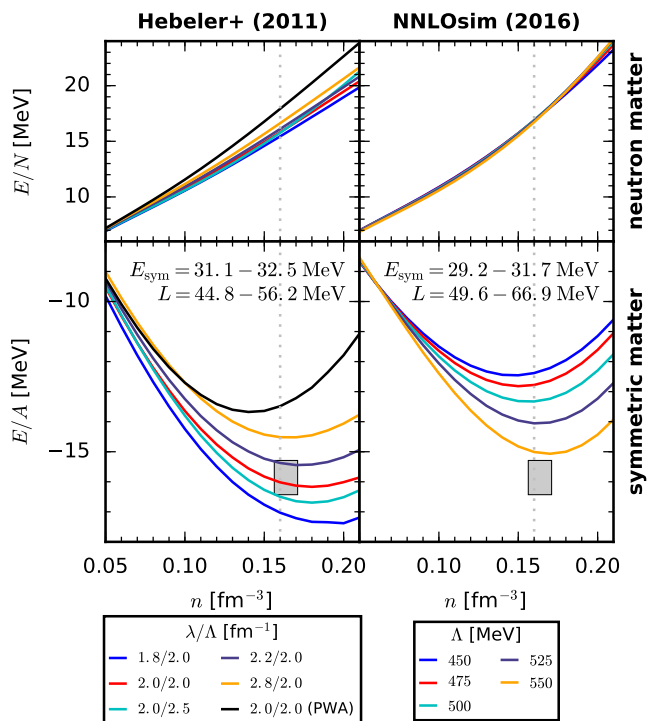


FIG. 1. (Color online) Energy per particle of neutron matter (top row) and symmetric nuclear matter (bottom row) based on the Hebeler+ [16] and NNLOsim [6] NN and 3N interactions (columns). Results are shown for λ/Λ_{3N} for the interactions of Ref. [16] and $\Lambda_{NN} = \Lambda_{3N}$ for those of Ref. [6]. For symmetric matter, the gray box denotes the saturation region, $n_0 = 0.164 \pm 0.007 \text{ fm}^{-3}$ and $E/A = -15.86 \pm 0.57 \text{ MeV}$. We also give the calculated range for the symmetry energy E_{sym} and its slope parameter L at $n_0 = 0.16 \text{ fm}^{-3}$ (indicated by the dashed vertical line).

Specifically, in this first application, we consider all contributions from NN interactions up to fourth order in MBPT (around the Hartree-Fock reference state). Contributions from 3N interactions are included exactly up to second order, including residual 3N-3N terms, which have only been evaluated so far for contact interactions [44]. At third order, we neglect all terms that involve at least one residual 3N contribution, whereas at fourth order we neglect all 3N contributions. These contributions turn out to be smaller (see discussion below). This amounts to 4, 20 = 3 · 2³ − 4, and 24 = 39 − 15 diagrams at second, third, and fourth order, respectively, with up to 21-dimensional momentum integrals per diagram. The number of diagrams at third (fourth) order can be reduced by 4 (15) at zero temperature. In comparison, a full calculation would involve 39 · 2⁴ = 624 fourth-order diagrams. We also evaluate the 4N Hartree-Fock energy, but it is generally small, in agreement with Ref. [18].

We assess the numerical convergence of the integration by varying the number of sampling points as well as employing two different Monte-Carlo algorithms [28], in

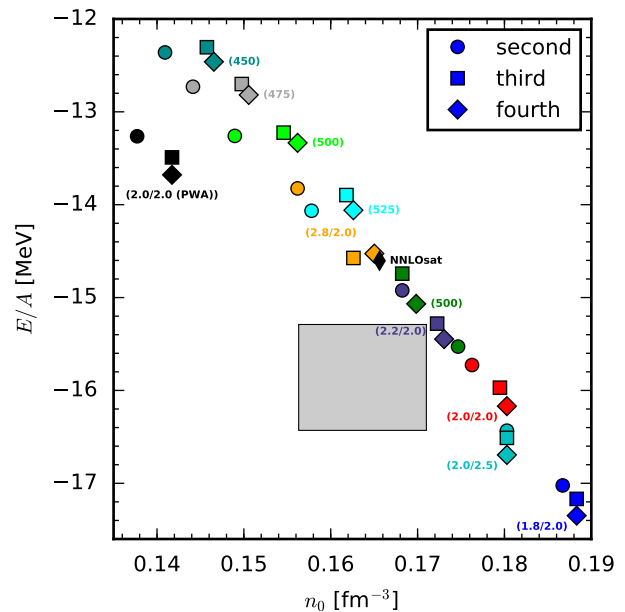


FIG. 2. (Color online) Correlation between the calculated saturation density n_0 and saturation energy E/A for the Hebeler+ [16] and NNLOsim [6] NN and 3N interactions obtained at second, third, and fourth order in MBPT. The values of λ/Λ_{3N} and $\Lambda_{NN} = \Lambda_{3N}$, as well as the saturation region are as in Fig. 1. The diamond refers to the NNLOsat result [1].

addition to the variance as statistical uncertainty. The framework is remarkably efficient due to performance optimization and parallelization. Most diagrams up to fourth order can be evaluated within about 10 minutes to a precision of $\lesssim 10 \text{ keV}$. The precise evaluation of a few specific third-order diagrams involving three 3N interactions requires more time due to the higher dimensionality of the momentum integrals. However, the strength of the present Monte-Carlo approach is that the precision can be controlled in a systematic way using the uncertainty estimates, as short runtimes are important when optimizing nuclear interactions. For this purpose, one could start constraining a fit with lower accuracy around the saturation point and then successively become more accurate.

Results for nuclear matter.— In Fig. 1 we present results for the energy per particle in symmetric nuclear matter and neutron matter based on the Hebeler+ [16] and NNLOsim [6] NN and 3N interactions up to fourth order in MBPT. For symmetric matter we show the empirical saturation region by a box with boundaries $n_0 = 0.164 \pm 0.007 \text{ fm}^{-3}$ and $E/A = -15.86 \pm 0.37 \pm 0.2 \text{ MeV}$ where the first uncertainties are as in Ref. [22] and we add an additional 0.2 MeV from Ref. [45]. In addition, we give results for symmetry energy range $E_{\text{sym}} = E/N - E/A$ as well as its slope parameter $L = 3n_0 \partial_n E_{\text{sym}}$ at $n_0 = 0.16 \text{ fm}^{-3}$. Both are predicted with narrow ranges.

The Hebeler+ interactions were obtained by a similarity renormalization group evolution [46] of the N³LO

TABLE I. Contributions to the energy per particle at $n_0 = 0.16 \text{ fm}^{-3}$ in symmetric nuclear matter at consecutive orders in MBPT based on the Hebeler+ [16] interaction with $\lambda/\Lambda = 1.8/2.0 \text{ fm}^{-1}$ and the N^2LO and N^3LO interactions of this work with Λ/c_D [for the central c_D fit value (black diamonds) in Fig. 4]. All energies are in MeV.

chiral order	Λ/c_D	second order			third order	fourth order	
		NN-only	NN+3N	3N res.	NN+3N	NN-only	NN+3N ^a
$\text{N}^3\text{LO}/\text{N}^2\text{LO}$	$\lambda/\Lambda = 1.8/2.0 \text{ fm}^{-1}$	-2.30	-2.24	-0.40	-0.10	-0.20	-0.07
N^2LO	450/+ 2.50	-6.23	-13.38	-0.42	-2.08	0.07	0.24
	500/- 1.50	-8.61	-14.49	-0.66	-0.77	0.32	0.75
N^3LO	450/+ 0.50	-8.93	-15.54	-0.38	-2.85	0.61	0.92
	500/- 3.00	-10.63	-14.65	-0.87	-1.00	0.65	1.10

^a Contributions from 3N forces at fourth order in MBPT are not included in our fits. These values here are an uncertainty estimate using normal-ordered 3N contributions in the $P = 0$ approximation (see Refs. [22, 25]).

NN potential of Ref. [47] to different resolution scales λ , whereas the 3N couplings c_D and c_E were fixed at these resolution scales by fits to the ${}^3\text{H}$ binding energy and the ${}^4\text{He}$ charge radius. Despite being fitted to only few-body data, these interactions are able to reproduce empirical saturation in Fig. 1 within uncertainties given by the band of the Hebeler+ interactions [16]. In addition, recent calculations of medium-mass and heavy nuclei based on some of these interactions show remarkable agreement with experimental data [2, 4, 8–10, 48] and thus offer new ab initio possibilities to investigate the nuclear chart.

The second column of Fig. 1 shows results for the NNLOsim potentials [6] (using $T_{\text{rel}} = 290 \text{ MeV}$) for different cutoff values (see legend). These interactions were obtained by a simultaneous fit of all low-energy couplings to two-body and few-body data. We observe a weak cut-off dependence for these potentials in neutron matter over the entire density range and in symmetric matter up to $n \lesssim 0.08 \text{ fm}^{-3}$. At higher densities, the variation of the energy per particle increases up to $\sim 3 \text{ MeV}$ at $n_0 = 0.16 \text{ fm}^{-1}$ with a very similar density dependence. Overall, all the NNLOsim interactions turn out to be too repulsive compared to the empirical saturation region.

We study the many-body convergence of the Hebeler+ and NNLOsim interactions by plotting in Fig. 2 the calculated saturation energy as a function of the calculated saturation density at second, third, and fourth order in MBPT. The annotated values denote the cutoff scales of the different potentials (see legend of Fig. 1). For all shown interactions, we observe a very good convergence in the many-body expansion, indicating that these chiral interactions are perturbative over this density regime. Moreover, we find a pronounced linear correlation band (similar to the Coester line [49] for NN potentials), which however overlaps with the empirical saturation region as 3N forces are included. Note that the Hebeler+ interaction that breaks most from the linear correlation is “2.0/2.0 (PWA)”, for which the c_i values in the 3N forces are significantly larger.

Finally, in Table I we show the hierarchy of contributions from second, third, and fourth order at $n_0 =$

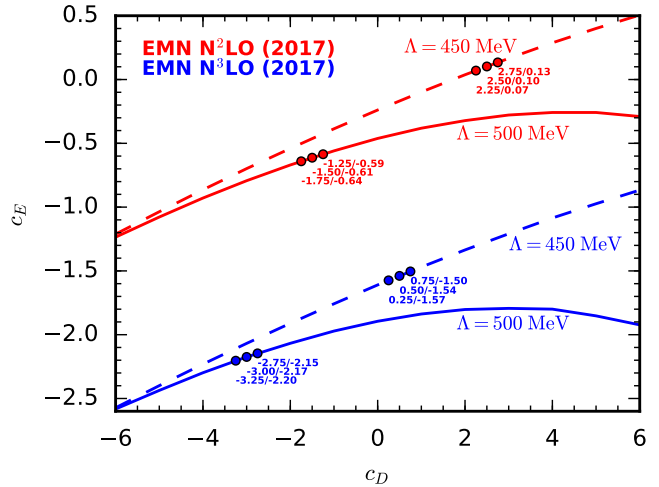


FIG. 3. (Color online) Three-nucleon couplings c_D and c_E that reproduce the ${}^3\text{H}$ binding energy using the EMN NN potentials of Ref. [39] with $\Lambda = 450 \text{ MeV}$ (dashed) and $\Lambda = 500 \text{ MeV}$ (solid line) at N^2LO (red) and N^3LO (blue) combined with consistent 3N interactions at these orders using $\Lambda_{3\text{N}} = \Lambda_{\text{NN}}$. The points (diamonds) on each line correspond to the fits to the empirical saturation region (see Fig. 4), while the annotated numbers give the corresponding values of c_D/c_E .

0.16 fm^{-3} for the Hebeler+ “1.8/2.0” interaction, which is most commonly used in the recent ab initio calculations of medium-mass and heavy nuclei. At second order, we give the contributions from NN interactions (NN-only), from NN plus 3N contributions that can be represented in form of a density-dependent NN interactions (NN+3N), and the residual 3N contribution (3N res.). We find that the residual 3N term is significantly smaller compared to the other contributions. This justifies that this contribution was usually neglected in previous calculations because it requires an explicit treatment of 3N forces in MBPT. However, note that this in general depends on details of the NN and 3N interactions [50, 51]. Furthermore, we find that the third-order contributions are significantly smaller than the second-order terms for all studied interactions. The fourth order contributions are particularly

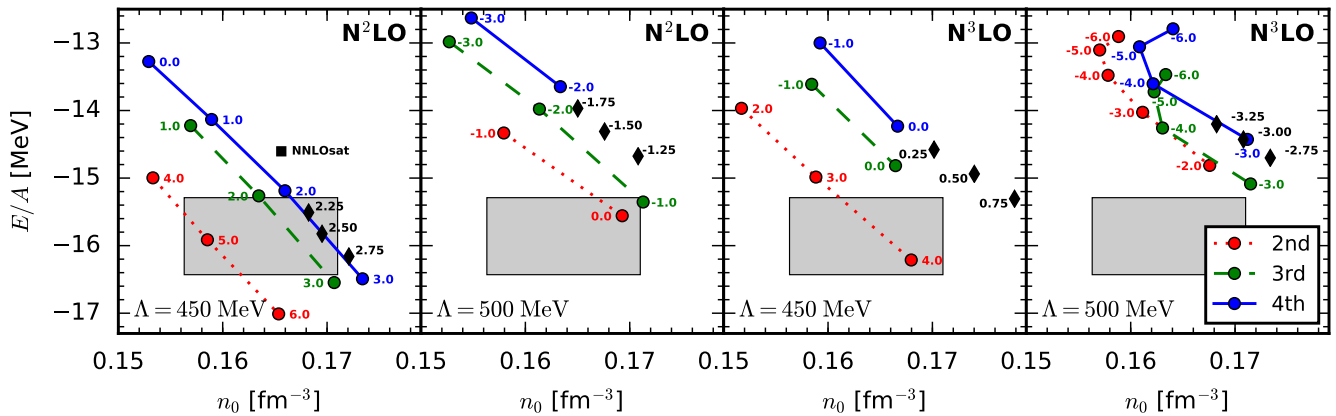


FIG. 4. (Color online) Saturation density and energy of symmetric nuclear matter at different orders in MBPT for the NN and 3N interactions at $N^2\text{LO}$ and $N^3\text{LO}$ of Fig. 3. The points are for different values of c_D (annotated numbers), while the red-dotted, green-dashed, and blue-solid lines correspond to calculations at second, third, and fourth order in MBPT. The left (right) two panels are for $N^2\text{LO}$ ($N^3\text{LO}$) with $\Lambda = 450$ MeV and $\Lambda = 500$ MeV. The diamonds in each panel represent the calculations with a simultaneous good reproduction of both saturation density and energy at fourth order in MBPT. The empirical saturation region is given by the gray box (see Fig. 1).

small for the “1.8/2.0” interaction, but also in the other cases smaller than the third-order contributions.

Fit to saturation region.— The observed convergence pattern indicates that the studied nonlocal interactions are sufficiently perturbative and allow calculations with controlled many-body uncertainties. This offers the possibility to use the new Monte-Carlo framework for constraining the 3N couplings using information from nuclear matter. In this Letter, we demonstrate this using the $N^2\text{LO}$ and $N^3\text{LO}$ NN potentials of Entem, Machleidt, and Nosyk (ENM) [39] with $\Lambda = 450$ MeV and $\Lambda = 500$ MeV, which are very promising also in terms of their Weinberg eigenvalues [52]. As a first step, we fit to the ^3H binding energy, which leads to a relation of the 3N couplings c_D and c_E shown in Fig. 3. For the fits, we include all 3N contributions consistently up to $N^2\text{LO}$ and $N^3\text{LO}$, respectively. The corresponding 3N matrix elements were computed as in Ref. [43]. We use $\Lambda_{3\text{N}} = \Lambda_{\text{NN}} = \Lambda$ and a nonlocal regulator of the form $f_\Lambda(p, q) = \exp[-((p^2 + 3/4q^2)/\Lambda^2)^4]$ for the Jacobi momenta p and q of the initial and final states [33]. For both cutoffs and chiral orders, we obtain c_E couplings of natural size in the wide c_D range explored.

As a second step, we calculate nuclear matter for the range of 3N couplings and determine the saturation point. In Fig. 4, we present the saturation points at $N^2\text{LO}$ and $N^3\text{LO}$ as a function of the c_D and at different orders in MBPT. Similar to the interactions shown in Fig. 2, we find a natural convergence pattern. Note that the shown points on the trajectories correspond to different c_D values at second order compared to third and fourth order. Contributions at third order are therefore more significant in these cases, whereas fourth-order corrections are again much smaller as is shown in Table I. In general, Fig. 4 demonstrates that it is possible to determine natu-

ral c_D/c_E combinations at $N^2\text{LO}$ and $N^3\text{LO}$ with reasonable saturation properties for both cutoff cases considered. However, with respect to our $N^2\text{LO}$ results, $N^3\text{LO}$ contributions provide slightly too much repulsion.

In each panel of Fig. 4, we mark the three couplings that provide a reasonable fit to the saturation region by black diamonds, whereas the actual c_D/c_E values are given in the annotations in Fig. 3. The resulting equations of state of symmetric nuclear matter and neutron matter at $N^2\text{LO}$ and $N^3\text{LO}$ are shown in Fig. 5. Note that only two lines are present in neutron matter since the shorter-range 3N interactions do not contribute [25]. For completeness, the calculated $N^3\text{LO}$ 4N Hartree-Fock energies at n_0 are ≈ 150 keV for both cutoffs, which is negligible compared to the overall uncertainty [18]. As for the Hebeler+ and NNLOsim results, the symmetry energy and the L parameter are predicted with a remarkably narrow range. In symmetric matter, we also observe a weak cutoff dependence at $N^3\text{LO}$, whereas the results for $\Lambda = 450$ MeV are clearly separated from $\Lambda = 500$ MeV at $N^2\text{LO}$, with the former achieving the best fits to the saturation region. Finally, we estimate the theoretical uncertainty from the chiral expansion following Ref. [38], using $Q = p/\Lambda_b$ with breakdown scale $\Lambda_b = 500$ MeV and average momentum $p = \sqrt{3/5} k_F$. The bands overlap from $N^2\text{LO}$ to $N^3\text{LO}$, and we clearly see that the theoretical uncertainties are significantly reduced at $N^3\text{LO}$.

Summary.— We have presented a new Monte-Carlo framework for calculations of nuclear matter, which allows to include higher order contributions from chiral interactions and is capable of going to high enough orders in the many-body expansion for suitable interactions. The new method was applied to the calculation of the symmetric-matter and neutron-matter energy in an

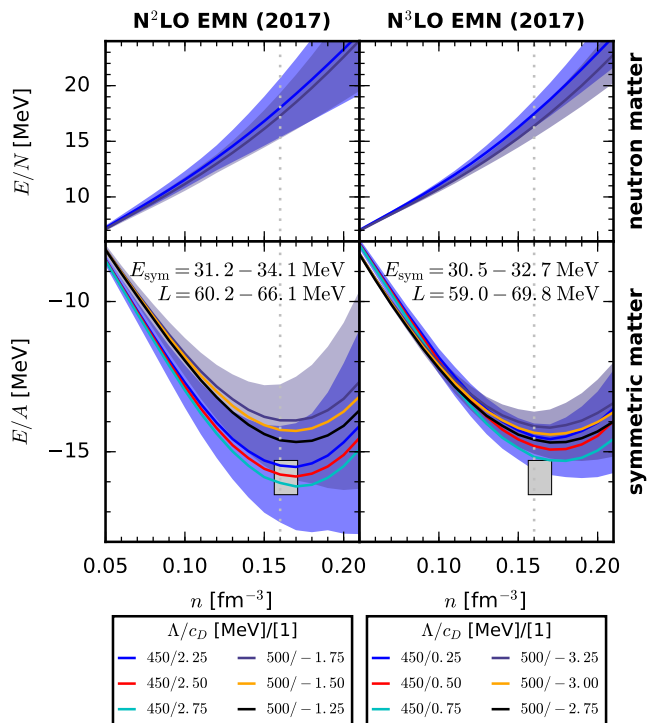


FIG. 5. (Color online) Energy per particle in neutron matter (top row) and symmetric nuclear matter (bottom row) based on chiral interactions at N^2 LO (first column) and N^3 LO (second column) fit to the empirical saturation region (see Fig. 4). The fits are labeled by Λ/c_D in the legend. As in Fig. 5, we also give the symmetry energy E_{sym} and its slope parameter L at each order. The blue ($\Lambda = 500$ MeV) and gray ($\Lambda = 450$ MeV) bands estimate the theoretical uncertainty following Ref. [38]. Note that the annotated results for E_{sym} and L do not include the latter uncertainty.

expansion around Hartree-Fock, but it can be easily generalized to expansions around other reference states. This enabled first benchmarks of chiral low-momentum interactions to fourth order in MBPT showing a systematic order-by-order convergence. We then used this to develop new chiral interactions at N^2 LO and N^3 LO, including NN, 3N, and 4N interactions at N^3 LO, where the 3N couplings are fit to the triton and to saturation properties. Our work shows that a good description of nuclear matter at these orders is possible, with a systematic behavior from N^2 LO to N^3 LO and natural low-energy couplings. Thanks to the computational efficiency, the new framework is also ideal for the incorporation of nuclear matter properties in the fitting of novel nuclear interactions. It will be exciting to see what these interactions predict for nuclei and for the equation of state for astrophysics.

We thank A. Ekström, B. Carlsson, C. Forssén, R. J. Furnstahl, and T. Hahn for useful discussions, and R. Machleidt for providing us with the EMN potentials. We also thank C. Iwainsky for helping us to optimize the code performance. This work was supported in part

by the European Research Council Grant No. 307986 STRONGINT and the Deutsche Forschungsgemeinschaft through Grant SFB 1245. Computational resources have been provided by the Lichtenberg high performance computer of the TU Darmstadt.

* Email: christian.drischler@physik.tu-darmstadt.de

† Email: kai.hebeler@physik.tu-darmstadt.de

‡ Email: schwenk@physik.tu-darmstadt.de

- [1] A. Ekström, G. R. Jansen, K. A. Wendt, G. Hagen, T. Papenbrock, B. D. Carlsson, C. Forssén, M. Hjorth-Jensen, P. Navrátil, and W. Nazarewicz, Phys. Rev. C **91**, 051301(R) (2015).
- [2] G. Hagen, A. Ekström, C. Forssén, G. R. Jansen, W. Nazarewicz, T. Papenbrock, K. A. Wendt, S. Bacca, N. Barnea, B. Carlsson, C. Drischler, K. Hebeler, M. Hjorth-Jensen, M. Miorelli, G. Orlandini, A. Schwenk, and J. Simonis, Nat. Phys. **12**, 186 (2016).
- [3] J. Simonis, K. Hebeler, J. D. Holt, J. Menéndez, and A. Schwenk, Phys. Rev. C **93**, 011302(R) (2016).
- [4] J. Simonis, S. R. Stroberg, K. Hebeler, J. D. Holt, and A. Schwenk, Phys. Rev. C **96**, 014303 (2017).
- [5] A. Ekström, G. Hagen, T. D. Morris, T. Papenbrock, and P. D. Schwartz, (2017), [arXiv:1707.09028](https://arxiv.org/abs/1707.09028).
- [6] B. D. Carlsson, A. Ekström, C. Forssén, D. F. Strömberg, G. R. Jansen, O. Lilja, M. Lindby, B. A. Mattsson, and K. A. Wendt, Phys. Rev. X **6**, 011019 (2016).
- [7] S. Binder, J. Langhammer, A. Calci, and R. Roth, Phys. Lett. B **736**, 119 (2014).
- [8] R. F. Garcia Ruiz, M. L. Bissell, K. Blaum, A. Ekström, N. Frömmgen, G. Hagen, M. Hammen, K. Hebeler, J. D. Holt, G. R. Jansen, M. Kowalska, K. Kreim, W. Nazarewicz, R. Neugart, G. Neyens, W. Nörtershäuser, T. Papenbrock, J. Papuga, A. Schwenk, J. Simonis, K. A. Wendt, and D. T. Yordanov, Nat. Phys. **12**, 594 (2016).
- [9] G. Hagen, G. R. Jansen, and T. Papenbrock, Phys. Rev. Lett. **117**, 172501 (2016).
- [10] T. D. Morris, J. Simonis, S. R. Stroberg, C. Stumpf, G. Hagen, J. D. Holt, G. R. Jansen, T. Papenbrock, R. Roth, and A. Schwenk, (2017), [arXiv:1709.02786](https://arxiv.org/abs/1709.02786).
- [11] G. Hagen, T. Papenbrock, A. Ekström, K. Wendt, G. Baardsen, S. Gandolfi, M. Hjorth-Jensen, and C. J. Horowitz, Phys. Rev. C **89**, 014319 (2014).
- [12] A. Gezerlis, I. Tews, E. Epelbaum, S. Gandolfi, K. Hebeler, A. Nogga, and A. Schwenk, Phys. Rev. Lett. **111**, 032501 (2013).
- [13] A. Roggero, A. Mukherjee, and F. Pederiva, Phys. Rev. Lett. **112**, 221103 (2014).
- [14] J. E. Lynn, I. Tews, J. Carlson, S. Gandolfi, A. Gezerlis, K. E. Schmidt, and A. Schwenk, Phys. Rev. Lett. **116**, 062501 (2016).
- [15] A. Carbone, A. Polls, and A. Rios, Phys. Rev. C **88**, 044302 (2013).
- [16] K. Hebeler, S. K. Bogner, R. J. Furnstahl, A. Nogga, and A. Schwenk, Phys. Rev. C **83**, 031301(R) (2011).
- [17] I. Tews, T. Krüger, K. Hebeler, and A. Schwenk, Phys. Rev. Lett. **110**, 032504 (2013).
- [18] T. Krüger, I. Tews, K. Hebeler, and A. Schwenk, Phys. Rev. C **88**, 025802 (2013).

- [19] J. W. Holt, N. Kaiser, and W. Weise, *Prog. Part. Nucl. Phys.* **73**, 35 (2013).
- [20] L. Coraggio, J. W. Holt, N. Itaco, R. Machleidt, L. E. Marcucci, and F. Sammarruca, *Phys. Rev. C* **89**, 044321 (2014).
- [21] C. Wellenhofer, J. W. Holt, N. Kaiser, and W. Weise, *Phys. Rev. C* **89**, 064009 (2014).
- [22] C. Drischler, K. Hebeler, and A. Schwenk, *Phys. Rev. C* **93**, 054314 (2016).
- [23] C. Drischler, A. Carbone, K. Hebeler, and A. Schwenk, *Phys. Rev. C* **94**, 054307 (2016).
- [24] J. W. Holt and N. Kaiser, *Phys. Rev. C* **95**, 034326 (2017).
- [25] K. Hebeler and A. Schwenk, *Phys. Rev. C* **82**, 014314 (2010).
- [26] J. W. Holt, N. Kaiser, and W. Weise, *Phys. Rev. C* **81**, 024002 (2010).
- [27] G. P. Lepage, *J. Comput. Phys.* **27**, 192 (1978).
- [28] T. Hahn, *Comput. Phys. Commun.* **168**, 78 (2005).
- [29] T. Hahn, *Comput. Phys. Commun.* **207**, 341 (2016).
- [30] P. D. Stevenson, *Int. J. Mod. Phys. C* **14**, 1135 (2003).
- [31] N. J. A. Sloane, <https://oeis.org/A064732>, the Encyclopedia of Integer Sequences: Number of labeled Hugenholtz diagrams with n nodes.
- [32] R. Machleidt and D. R. Entem, *Phys. Rep.* **503**, 1 (2011).
- [33] E. Epelbaum, A. Nogga, W. Glöckle, H. Kamada, U.-G. Meißner, and H. Witała, *Phys. Rev. C* **66**, 064001 (2002).
- [34] V. Bernard, E. Epelbaum, H. Krebs, and U.-G. Meißner, *Phys. Rev. C* **77**, 064004 (2008).
- [35] V. Bernard, E. Epelbaum, H. Krebs, and U.-G. Meißner, *Phys. Rev. C* **84**, 054001 (2011).
- [36] E. Epelbaum, *Phys. Lett. B* **639**, 456 (2006).
- [37] E. Epelbaum, H. Krebs, and U.-G. Meißner, *Phys. Rev. Lett.* **115**, 122301 (2015).
- [38] E. Epelbaum, H. Krebs, and U.-G. Meißner, *Eur. Phys. J. A* **51**, 53 (2015).
- [39] D. R. Entem, R. Machleidt, and Y. Nosyk, *Phys. Rev. C* **96**, 024004 (2017).
- [40] H. Krebs, A. Gasparyan, and E. Epelbaum, *Phys. Rev. C* **85**, 054006 (2012).
- [41] H. Krebs, A. Gasparyan, and E. Epelbaum, *Phys. Rev. C* **87**, 054007 (2013).
- [42] D. R. Entem, N. Kaiser, R. Machleidt, and Y. Nosyk, *Phys. Rev. C* **92**, 064001 (2015).
- [43] K. Hebeler, H. Krebs, E. Epelbaum, J. Golak, and R. Skibinski, *Phys. Rev. C* **91**, 044001 (2015).
- [44] N. Kaiser, *Eur. Phys. J. A* **48**, 58 (2012).
- [45] G. F. Bertsch and D. Bingham, (2017), [arXiv:1703.08844](https://arxiv.org/abs/1703.08844).
- [46] S. K. Bogner, R. J. Furnstahl, and A. Schwenk, *Prog. Part. Nucl. Phys.* **65**, 94 (2010).
- [47] D. R. Entem and R. Machleidt, *Phys. Rev. C* **68**, 041001(R) (2003).
- [48] J. Birkhan, M. Miorelli, S. Bacca, S. Bassauer, C. A. Bertulani, G. Hagen, H. Matsubara, P. von Neumann-Cosel, T. Papenbrock, N. Pietralla, V. Y. Ponomarev, A. Richter, A. Schwenk, and A. Tamii, *Phys. Rev. Lett.* **118**, 252501 (2017).
- [49] F. Coester, *Nucl. Phys.* **7**, 421 (1958).
- [50] A. Dyhdalo, R. J. Furnstahl, K. Hebeler, and I. Tews, *Phys. Rev. C* **94**, 034001 (2016).
- [51] A. Dyhdalo, S. K. Bogner, and R. J. Furnstahl, (2017), [arXiv:1707.07199](https://arxiv.org/abs/1707.07199).
- [52] J. Hoppe, C. Drischler, R. J. Furnstahl, K. Hebeler, and A. Schwenk, (PRC in press), [arXiv:1707.06438](https://arxiv.org/abs/1707.06438).